Scattering by circularly symmetric structured optical fields in stratified media

Jungho Mun,[1,*] Hongyoon Kim,[1] Seong-Won Moon,[1] and Junsuk Rho[1,2,†]

[1]*Department of Mechanical Engineering, Pohang University of Science and Technology, Pohang 37673, Republic of Korea*

[2]*Department of Chemical Engineering, Pohang University of Science and Technology, Pohang 37673, Republic of Korea*

(Received 1 September 2022; revised 26 October 2022; accepted 1 November 2022; published 16 November 2022)

Structured optical fields (SOFs) with spatially inhomogeneous phase, amplitude, or polarization can excite substantially different optical responses in nanoscale scattering particles. Inhibition of low-order multipolar resonances, excitation of dark modes and anapoles, and spin and orbital angular momenta dichroism have been demonstrated, broadening the scope of nanoscale manipulations of optical resonances by using these engineered external SOFs. However, studying scattering effects illuminated by SOFs is more complicated than conventional plane wave illuminations, and the difficulty increases for scattering particles on a substrate. In this paper, we present explicit expressions of SOFs propagating through stratified media, or multilayered systems, and provide their beam-shape coefficients. Specifically, simple analytic expressions are provided for circularly symmetric Bessel beams passing through an interface. Then, scattering calculations for a dielectric sphere on a substrate illuminated by an evanescent optical vortex are performed via the *T*-matrix method, which yields accurate and efficient results as compared with finite element analysis. This paper will find practical applications in modeling SOFs for realistic configurations of scattering of particles on a substrate at nonplanar nonparaxial external light source illuminations.

DOI: 10.1103/PhysRevB.106.184414

I. INTRODUCTION

Subwavelength resonant particles are powerful tools for manipulating light-matter interactions. By engineering the shape and material of the particles and their arrangements, many intriguing optical effects have been conceived including artificial optical magnetism, nonradiating anapoles, directional scattering [1], and electromagnetic chirality [2]. Due to the subwavelength size of the scattering particles, the underlying physics of the optical phenomena are often interpreted as pointlike multipole sources. In this framework, exotic optical phenomena are often relevant to the excitation and radiation of higher-order multipoles and their interferences, which have been achieved by structured particles with peculiar morphologies typically under plane wave illuminations.

Recent achievements in the generation and control of structured lights [3] using spatial light modulators, digital micromirror devices, and metasurfaces would extend the light-matter interactions in metaphotonics. Some widely studied structured optical fields (SOFs) include tightly focused optical beams with localized hotspots and strong longitudinal polarization component [4], optical vortex beams with helical phase fronts and singularity of phase and amplitude [5], and cylindrical vector beams with rotating polarization states [6]. Such SOFs with spatially inhomogeneous amplitude, phase, or polarization states provide diverse optical effects arising from engineered multipole excitations. For instance, SOFs with well-defined spin and orbital angular momenta can excite dark modes [7,8] and anapoles [9] that cannot be probed using ordinary plane waves due to the selection rule [10]. Also, the inhibition of low-order multipoles and the selective excitation of higher-order multipoles [11,12] and the angular momentum dichroisms [13,14] have been exploited. Similarly, cylindrical vector beams have demonstrated excitations of toroidal dipoles [15], anapoles [16–18], quasibound states [19], as well as selective excitation of multipole resonances [20]. In addition, evanescent fields with extraordinary spin and momenta [21] may offer unconventional optomechanical manipulations. For these potentials, light-matter interactions between SOFs and structured particles are actively researched.

To study these problems, accurate descriptions of SOFs, as well as the particles, are required, and the *T*-matrix method based on a multipole framework can be an accurate and efficient approach for scattering problems. First, to accurately describe nonparaxial optical fields, vector angular spectrum representation is widely utilized, which remodels the optical field as a sum of partial plane waves [22]. The resulting optical fields exactly satisfy Maxwell's equations and therefore can be multipole decomposed for scattering problems [23–26]. Recently, expressions of Bessel beams [27,28] and their multipole expansions [29] were reported.

In this paper, we provide explicit expressions of circularly symmetric SOFs in stratified media. The optical fields are exact Maxwellian fields modeled using the vector angular spectrum representation, and the expression of their multipole expansions is provided for scattering problems. Scattering calculations for a dielectric sphere illuminated by an evanescent optical vortex are demonstrated, and compared against

*mjh92@postech.ac.kr
†jsrho@postech.ac.kr

 ©2022 American Physical Society

finite element analysis. Superior numerical efficiency of the semianalytic T-matrix method is confirmed, which can be applied to parametric studies and optimization problems. Far-field calculations are also demonstrated for the scattering of a particle on a substrate. This paper demonstrates the T-matrix method as a promising tool for studying fundamental physics and solving engineering problems for scattering in stratified media.

II. CIRCULARLY SYMMETRIC OPTICAL FIELDS

First, we discuss the formulation of SOFs in free space. Paraxial beam models, such as paraxial Laguerre-Gaussian beams [30], have widely been used to approximate SOFs, but the error due to the paraxial approximation can be large for strongly nonparaxial optical fields, such as tightly focused beams. This paraxial error is especially large near the focal point, which is usually the region of interest. Formulation of exact optical fields is crucial for scattered field calculation, because the paraxial error can be captured in scattered fields, causing erroneous results. Exact Maxwellian SOFs are modeled using the vector angular spectrum representation that expresses the optical fields as a sum of partial plane waves as [22] $\mathbf{E}(\mathbf{r}) = E_0 \int_{\mathbb{R}^2} d^2\mathbf{k}_\parallel g(\mathbf{k}_\parallel)\mathbf{e}(\mathbf{k}_\parallel)e^{i\mathbf{k}\cdot\mathbf{r}}$, where the integration is performed over k space as $d^2\mathbf{k}_\parallel = dk_x dk_y$, $g(\mathbf{k}_\parallel)$ is the angular spectrum or the weight of partial plane waves, and $\mathbf{e}(\mathbf{k}_\parallel)$ is the complex unit polarization vector of partial plane waves. By noting that $k_x = k\sin\alpha\cos\beta$, $k_y = k\sin\alpha\sin\beta$, and $dk_x dk_y = k^2\cos\alpha\sin\alpha d\alpha d\beta$, the optical fields can be evaluated as

$$\mathbf{E}(\mathbf{r}) = E_0 \int d\alpha \sin\alpha w(\alpha) e^{ik_z z} \int_0^{2\pi} d\beta e^{il\beta} e^{i\mathbf{k}_\parallel\cdot\mathbf{r}} \times \sum_{q=p,s} A_q(\beta)\mathbf{e}_q(\alpha,\beta). \tag{1}$$

Here, circularly symmetric SOFs with their beam weights of the form $w(\alpha,\beta) = w(\alpha)e^{il\beta}$ are considered, where l is the topological charge of the SOFs. The polarization modes are split into p and s modes, or TM and TE modes with respect to the multilayers. The unit polarization vectors are $\mathbf{e}_p(\alpha,\beta) = [\cos\alpha\cos\beta, \cos\alpha\sin\beta, -\sin\alpha]^T$ and $\mathbf{e}_s(\alpha,\beta) = [-\sin\beta, \cos\beta, 0]^T$. The polarization weights $A_p(\beta) = p_x\cos\beta + p_y\sin\beta$ and $A_s(\beta) = -p_x\sin\beta + p_y\cos\beta$ are considered, where p_x and p_y denote the polarization states in the paraxial limit. Under this definition, circularly polarized states with $(p_x, p_y) = (1, \pm i)/\sqrt{2}$ can also be considered. Note that $A_p\mathbf{e}_p + A_s\mathbf{e}_s$ is the complex polarization vector found in the Debye-Wolf vector diffraction theory, so the expressions given in this paper can easily be extended to the optical fields modeled by the Debye-Wolf theory with an appropriate choice of $w(\alpha)$.

Equation (1) can be simplified by eliminating the integration with respect to β as

$$\mathbf{E}(\mathbf{r}) = E_0 \int d\alpha \sin\alpha w(\alpha) e^{ik_z z} \sum_{q=p,s} \tilde{\mathbf{e}}_q(\alpha), \tag{2}$$

where the partial cylindrical waves $\tilde{\mathbf{e}}_q(\alpha) = \int_0^{2\pi} d\beta e^{il\beta} e^{i\sigma\cos(\beta-\phi)} A_q(\beta)\mathbf{e}_q(\alpha,\beta)$ are evaluated as

$$\tilde{\mathbf{e}}_p(\alpha) = \pi i^l e^{il\phi} \begin{bmatrix} \cos\alpha[p_x J_l(\sigma) - p_+ e^{2i\phi} J_{l+2}(\sigma) - p_- e^{-2i\phi} J_{l-2}(\sigma)] \\ \cos\alpha[p_y J_l(\sigma) + ip_+ e^{2i\phi} J_{l+2}(\sigma) - ip_- e^{-2i\phi} J_{l-2}(\sigma)] \\ -2i\sin\alpha[p_+ e^{i\phi} J_{l+1}(\sigma) - p_- e^{-i\phi} J_{l-1}(\sigma)] \end{bmatrix},$$
$$\tilde{\mathbf{e}}_s(\alpha) = \pi i^l e^{il\phi} \begin{bmatrix} p_x J_l(\sigma) + p_+ e^{2i\phi} J_{l+2}(\sigma) + p_- e^{-2i\phi} J_{l-2}(\sigma) \\ p_y J_l(\sigma) - ip_+ e^{2i\phi} J_{l+2}(\sigma) + ip_- e^{-2i\phi} J_{l-2}(\sigma) \\ 0 \end{bmatrix}. \tag{3}$$

Here, the integral identities of Bessel functions $\int_0^{2\pi} e^{in\beta} e^{ix\cos\beta} d\beta = 2\pi i^n J_n(x)$ and $\mathbf{k}_\parallel\cdot\mathbf{r} = \sigma\cos(\beta-\phi)$ were used; $\sigma = k\rho\sin\alpha$, $\mathbf{r} = (\rho,\phi,z)$ in the cylindrical coordinate system, and $p_\pm = (p_x \mp ip_y)/2$. Note that the addition of these two results has the same functional form as the circularly symmetric SOFs in free space [26–28]. Partial cylindrical waves of cylindrical vector beams are provided in Appendix A.

The SOFs discussed in this paper are Maxwellian, and therefore can be exactly multipole decomposed. The multipole coefficients of SOFs, or the beam-shape coefficients (BSCs), are necessary for further scattering calculations. SOFs in free space and their BSCs have widely been studied including tightly focused laser beams [22,23], circularly symmetric Bessel beams [27–29], and cylindrical vector beams [26]. Refer to Appendix B for details on multipole expansion.

III. STRUCTURED OPTICAL FIELDS IN STRATIFIED MEDIA

Now, we discuss SOFs in stratified media, which can describe many realistic scattering configurations including particles on a substrate, on a spacer, and inside a finite layer. Because we consider optical fields as a sum of partial plane waves, SOFs in stratified media can be formulated by considering the propagation of each partial plane wave comprising the SOFs. The plane wave propagation in stratified media has been treated using the transfer matrix formulation. Then, SOFs in a layer can be expressed as

$$\mathbf{E}(\mathbf{r}) = E_0 \int d\alpha \sin\alpha w(\alpha) \int_0^{2\pi} d\beta e^{il\beta} e^{i\mathbf{k}_\parallel\cdot\mathbf{r}} \times \sum_{q=p,s} \left[c_{iq}\mathbf{e}_q e^{ik_{iz}z'} + c_{iq}^{(-)}\mathbf{e}_q^{(-)} e^{-ik_{iz}z'} \right], \tag{4}$$

where $k_{iz} = n_i k_0 \cos\alpha_i$, $z' = z - z_i$, z_i is the reference z coordinate of the layer, the subscript i denotes the layer index, and the superscript $(-)$ denotes backward propagating or reflected waves. The mode amplitudes c_{iq} are obtained from the transfer matrix calculations using the incident amplitudes A_q introduced in the previous section.

Noting that the plane wave propagation in the stratified media depends on the inclination angle α with respect to the layers and polarization modes p and s and is independent of β, the mode amplitudes can be expressed as $c_{iq}(\alpha,\beta) = \tilde{c}_{iq}(\alpha)A_q(\beta)$, where $\tilde{c}_{iq}$ is obtained using the unit incident amplitude. By performing analytic integration with respect to β as the previous section, the optical fields can be expressed in simple forms using the partial cylindrical waves. Then, SOFs in a layer are expressed as

$$\mathbf{E}(\mathbf{r}) = E_0 \int d\alpha \sin\alpha w(\alpha) \times \sum_{q=p,s} \left[\tilde{c}_{iq}\tilde{\mathbf{e}}_q(\alpha_i)e^{ik_{iz}z'} + \tilde{c}_{iq}^{(-)}\tilde{\mathbf{e}}_q^{(-)}(\alpha_i)e^{-ik_{iz}z'}\right], \quad (5)$$

where the backward propagating partial cylindrical waves are $\tilde{\mathbf{e}}_p^{(-)} = [(\tilde{e}_p)_x, (\tilde{e}_p)_y, -(\tilde{e}_p)_z]^T$ and $\tilde{\mathbf{e}}_s^{(-)} = \tilde{\mathbf{e}}_s$. Note that this simplification is only applicable for normally incident circularly symmetric SOFs.

We provide simple demonstrations of SOFs propagating through stratified media using Laguerre-Gaussian beams [Figs. 1(a) and 1(b)]. A Laguerre-Gaussian beam has its beam weight $w(\alpha) = \frac{k^2 w_0^2}{4\pi}\mathrm{LG}_{hl}(\frac{kw_0}{2}\sin\alpha)$, where $\mathrm{LG}_{hl}(x) = (\sqrt{2}x)^{|l|}L_h^{|l|}(2x^2)e^{-x^2}$, w_0 is the beam waist radius, $L_h^l(x)$ is the associated Laguerre polynomial, and the subscript h is the radial index related to the number of radial fringes, and we only consider the $h = 0$ case without any radial fringes. As an example, we consider the propagation of SOFs through a Fabry-Pérot resonator [Figs. 1(a) and 1(b)]. At the Fabry-Pérot resonant condition, total transmission is expected for plane waves or collimated beams [Fig. 1(a)], but focused beams exhibit nonunity transmission [31], because tightly focused SOFs including obliquely propagating partial plane waves reflect. This reflection is pronounced by the interference patterns in the substrate side [Fig. 1(b)]. This nonunity transmission of the focused beam can also be observed in its transmittance spectra [Fig. 1(c)], which is obtained by numerically integrating the Poynting vector in the superstrate.

Because the optical fields in a layer is a superposition of forward and backward propagating waves, their BSCs can be obtained as a slightly more complex form compared to the free space case with only forward propagating waves. BSCs of SOFs in a layer [Eq. (5)] are obtained as

$$\begin{aligned}\begin{bmatrix} a_{nm}^{\mathrm{e}} \\ a_{nm}^{\mathrm{m}} \end{bmatrix} &= -8\pi^2\gamma_{nm} i^{l+n-m+1} e^{i(l-m)\phi_p} \int d\alpha \sin\alpha w(\alpha) \\ &\times \left\{ p_+ e^{i\phi_p} J_{l-m+1}(\sigma_p) \begin{bmatrix} e^{ik_{iz}z'_p}[\tilde{c}_{is}\pi_{nm}(\alpha_i) + \tilde{c}_{ip}\tau_{nm}(\alpha_i)] + (-1)^{n+m}e^{-ik_{iz}z'_p}[\tilde{c}_{is}^{(-)}\pi_{nm}(\alpha_i) + \tilde{c}_{ip}^{(-)}\tau_{nm}(\alpha_i)] \\ e^{ik_{iz}z'_p}[\tilde{c}_{is}\tau_{nm}(\alpha_i) + \tilde{c}_{ip}\pi_{nm}(\alpha_i)] - (-1)^{n+m}e^{-ik_{iz}z'_p}[\tilde{c}_{is}^{(-)}\tau_{nm}(\alpha_i) + \tilde{c}_{ip}^{(-)}\pi_{nm}(\alpha_i)] \end{bmatrix} \right. \\ &\left. + p_- e^{-i\phi_p} J_{l-m-1}(\sigma_p) \begin{bmatrix} e^{ik_{iz}z'_p}[\tilde{c}_{is}\pi_{nm}(\alpha_i) - \tilde{c}_{ip}\tau_{nm}(\alpha_i)] + (-1)^{n+m}e^{-ik_{iz}z'_p}[\tilde{c}_{is}^{(-)}\pi_{nm}(\alpha_i) - \tilde{c}_{ip}^{(-)}\tau_{nm}(\alpha_i)] \\ e^{ik_{iz}z'_p}[\tilde{c}_{is}\tau_{nm}(\alpha_i) - \tilde{c}_{ip}\pi_{nm}(\alpha_i)] - (-1)^{n+m}e^{-ik_{iz}z'_p}[\tilde{c}_{is}^{(-)}\tau_{nm}(\alpha_i) - \tilde{c}_{ip}^{(-)}\pi_{nm}(\alpha_i)] \end{bmatrix} \right\}, \end{aligned} \quad (6)$$

where $\gamma_{nm} = \sqrt{\frac{(2n+1)(n-m)!}{4\pi n(n+1)(n+m)!}}$, $\pi_{nm}(\alpha) = \frac{m}{\sin\alpha}P_n^m(\cos\alpha)$, $\tau_{nm}(\alpha) = \frac{d}{d\alpha}P_n^m(\cos\alpha)$, $P_n^m(x)$ is the associated Legendre polynomial, $\sigma_p = \rho_p k_1 \sin\alpha_1$, and $z'_p = z_p - z_i$. The particle is located at an arbitrary position inside the layer $\mathbf{r}_p = (\rho_p, \phi_p, z_p)$ in the cylindrical coordinate system assuming that the beam center is at the origin.

IV. STRUCTURED OPTICAL FIELDS PASSING THROUGH AN INTERFACE

We further consider a simpler configuration of a SOF passing through a single interface divided by two infinite half spaces, where incident and reflected waves exist in the substrate ($z < 0$), and only forward propagating waves exist in the superstrate ($z > 0$). In this configuration, each partial plane wave comprising the SOF experiences Fresnel refraction, so the mode amplitude coefficients are given by the Fresnel coefficients. The incident, reflected, and transmitted fields are obtained as

$$\begin{aligned} \mathbf{E}_{\mathrm{inc}}(\mathbf{r}) &= E_0 \int d\alpha \sin\alpha w(\alpha)[\tilde{\mathbf{e}}_p(\alpha_1) + \tilde{\mathbf{e}}_s(\alpha_1)]e^{ik_{1z}z}, \\ \mathbf{E}_{\mathrm{ref}}(\mathbf{r}) &= E_0 \int d\alpha \sin\alpha w(\alpha)\left[r_p\tilde{\mathbf{e}}_p^{(-)}(\alpha_1) + r_s\tilde{\mathbf{e}}_s^{(-)}(\alpha_1)\right]e^{-ik_{1z}z}, \\ \mathbf{E}_{\mathrm{tra}}(\mathbf{r}) &= E_0 \int d\alpha \sin\alpha w(\alpha)[t_p\tilde{\mathbf{e}}_p(\alpha_2) + t_s\tilde{\mathbf{e}}_s(\alpha_2)]e^{ik_{2z}z}. \end{aligned} \quad (7)$$

The Fresnel coefficients are given as $t_p = \frac{2n_1\cos\alpha_1}{n_1\cos\alpha_2 + n_2\cos\alpha_1}$, $r_p = \frac{n_1\cos\alpha_2 - n_2\cos\alpha_1}{n_1\cos\alpha_2 + n_2\cos\alpha_1}$, $t_s = \frac{2n_1\cos\alpha_1}{n_1\cos\alpha_1 + n_2\cos\alpha_2}$, and $r_s = \frac{n_1\cos\alpha_1 - n_2\cos\alpha_2}{n_1\cos\alpha_1 + n_2\cos\alpha_2}$, where n_1 and n_2 are the refractive indices of substrate and superstrate, respectively. $\alpha_1 = \alpha$ is the incident angle in the substrate, and the refracted angle in the superstrate α_2 is obtained from Snell's law $n_1\sin\alpha_1 = n_2\sin\alpha_2$. This single interface case will find many useful applications, because this configuration is often encountered in scattering of particles on substrate or metasurfaces.

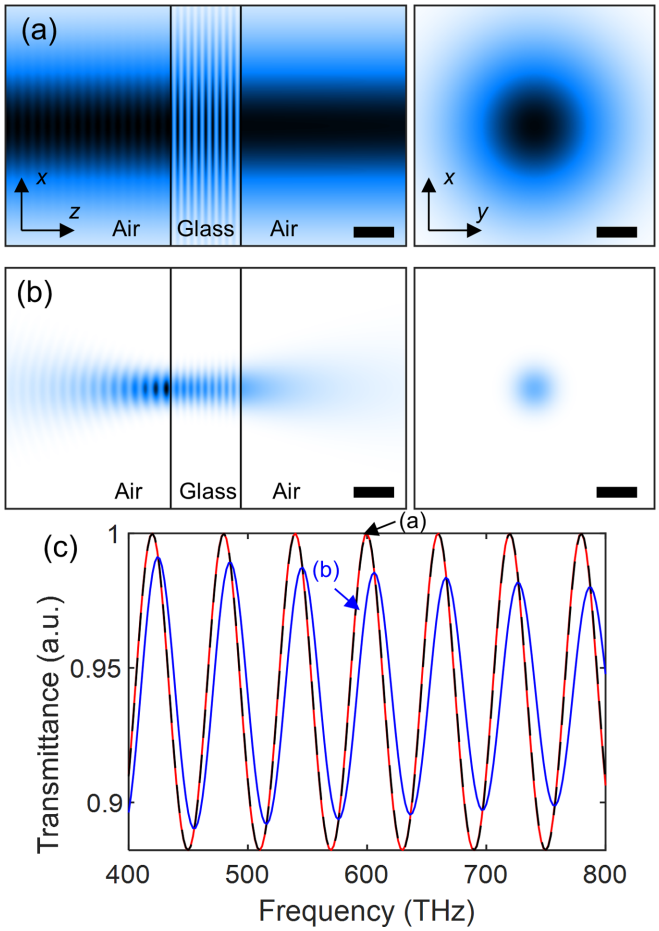

FIG. 1. Gaussian beams passing through a Fabry-Pérot resonator, inserted from left to right. (a), (b) The near-field distributions of (a) collimated ($w_0 = 6\lambda_0$) and (b) focused ($w_0 = \lambda_0$) Gaussian beams at $\lambda_0 = 0.5\,\mu\text{m} \approx 600\,\text{THz}$. (c) Transmittance spectra of the collimated (black) and focused (blue) Gaussian beams and plane wave (red). The refractive index of glass substrate is 1.43, and the interfaces are illustrated by black solid lines. Scale bar: $1\,\mu\text{m} = 2\lambda_0$.

For further simplicity, we consider a circularly symmetric Bessel beam with its weight given as $w(\alpha, \beta) = \frac{1}{\pi(1+\cos\alpha)} \frac{\delta(\alpha-\alpha_0)}{\sin\alpha} e^{il\beta}$, where the delta function eliminates the integration with respect to α, and α_0 is the inclination angle of the Bessel beam. In other words, a Bessel beam consists of partial plane waves propagating in a cone angled at α_0. The incident, reflected, and transmitted electric fields of a circularly symmetric Bessel beam are obtained as

$$\begin{aligned}
\mathbf{E}_{\text{inc}}(\mathbf{r}) &= \frac{E_0}{\pi(1+\cos\alpha_0)}[\tilde{\mathbf{e}}_p(\alpha_1) + \tilde{\mathbf{e}}_s(\alpha_1)]e^{ik_{1z}z}, \\
\mathbf{E}_{\text{ref}}(\mathbf{r}) &= \frac{E_0}{\pi(1+\cos\alpha_0)}\left[r_p\tilde{\mathbf{e}}_p^{(-)}(\alpha_1) + r_s\tilde{\mathbf{e}}_s^{(-)}(\alpha_1)\right]e^{-ik_{1z}z}, \\
\mathbf{E}_{\text{tra}}(\mathbf{r}) &= \frac{E_0}{\pi(1+\cos\alpha_0)}[t_p\tilde{\mathbf{e}}_p(\alpha_2) + t_s\tilde{\mathbf{e}}_s(\alpha_2)]e^{ik_{2z}z}. \qquad (8)
\end{aligned}$$

This simple analytic expression can describe various kinds of SOFs, which we briefly demonstrate below. First, optical vortices with inhomogeneous phase distribution and well-defined topological charge l can be described [Fig. 2(a)]. Optical vortices have rotating phase distribution around their beam axis. Due to its phase singularity at the beam center, the amplitude of the transverse part of the fields becomes zero and the characteristic doughnut-shaped beam is formed. Cylindrical vector beams with inhomogeneous polarization distribution can also be implemented [Fig. 2(b)]. Cylindrical vector beams have rotating polarization distribution around their beam axis, and special cases include radially and azimuthally polarized beams.

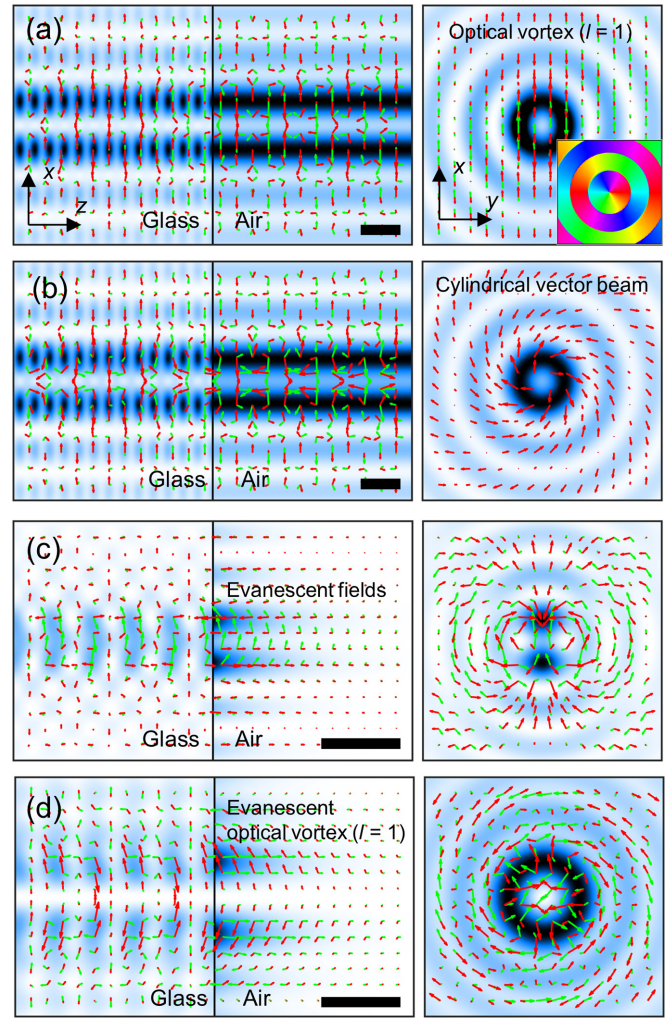

FIG. 2. Structured Bessel beams passing through an interface. Left panels show the xOz plane and right panels show the xy plane at $z = 100\,\text{nm}$. (a) Vortex Bessel beam with $(p_x, p_y) = (1, 0)$, $l = 1$, and $a_0 = 20^\circ$. The inset shows the phase of E_x. (b) Cylindrical vector Bessel beam with $(p_\rho, p_\phi) = (1, 1)$, $l = 0$, and $a_0 = 20^\circ$. (c) Evanescent Bessel beam with $(p_x, p_y) = (1, 0)$, $l = 0$, and $a_0 = 45^\circ$. (d) Evanescent vortex Bessel beam with $(p_x, p_y) = (1, i)/\sqrt{2}$, $l = 1$, and $a_0 = 45^\circ$. Red and green arrows illustrate electric field vectors with $\pi/2$ phase difference. Scale bar: $1\,\mu\text{m} = \lambda_0$.

Compared to free space propagation, SOFs passing through an interface can consider evanescent fields, which arise when waves propagate from a layer with a higher refractive index to a layer with a lower one at an incident angle exceeding the critical angle. For instance, an evanescent Bessel beam consisting of partial plane waves with the

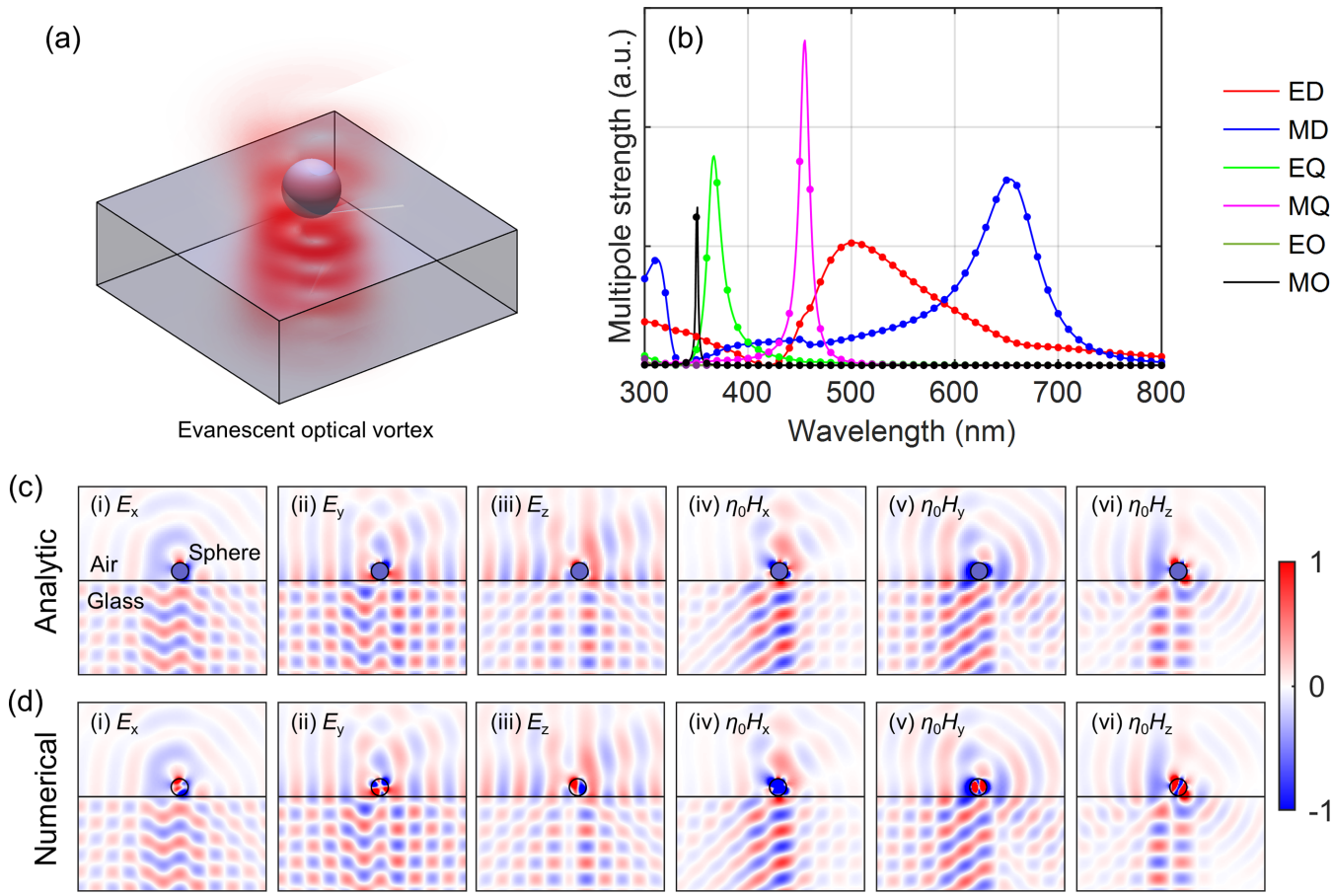

FIG. 3. Benchmark of scattering of a sphere on substrate illuminated by an evanescent optical vortex. (a) Schematic illustration of the scattering configuration. (b) Multipole-decomposed scattering cross sections calculated semianalytically and numerically with finite element analysis. (c), (d) Near fields calculated at $\lambda_0 = 350$ nm (c) semianalytically and (d) numerically with FEM. The incident SOF is an evanescent vortex Bessel beam with $l = 1$, $\alpha_0 = 45^\circ$, and polarization state $(p_x, p_y) = (1, i)/\sqrt{2}$; the sphere has refractive index 3.5, positioned at $\mathbf{r}_p = (80\,\text{nm}, 50\,\text{nm}, 100\,\text{nm})$.

inclination angle exceeding the critical angle can be described [Fig. 2(c)]. An exponential decrease in field intensity can be observed in the superstrate. Interestingly, the field amplitude maximum does not occur at the beam center. In fact, the electric field distribution in the xy plane resembles that of a dipole with two poles. Finally, a complicated SOF of an evanescent optical vortex can be described [Fig. 2(d)]. An evanescent optical vortex can trap particles and make them revolve around the beam axis [32].

BSCs of circularly symmetric Bessel beams in the superstrate [Eq. (9)] are obtained as

$$\begin{bmatrix} a^{\mathrm{e}}_{nm} \\ a^{\mathrm{m}}_{nm} \end{bmatrix} = -\frac{8\pi\gamma_{nm}}{1+\cos\alpha_0} i^{l+n-m+1} e^{i(l-m)\phi_p} e^{ik_{2z}z_p} \times \left\{ p_+ e^{i\phi_p} J_{l-m+1}(\sigma_p) \begin{bmatrix} t_s\pi_{nm}(\alpha_2) + t_p\tau_{nm}(\alpha_2) \\ t_s\tau_{nm}(\alpha_2) + t_p\pi_{nm}(\alpha_2) \end{bmatrix} + p_- e^{-i\phi_p} J_{l-m-1}(\sigma_p) \begin{bmatrix} t_s\pi_{nm}(\alpha_2) - t_p\tau_{nm}(\alpha_2) \\ t_s\tau_{nm}(\alpha_2) - t_p\pi_{nm}(\alpha_2) \end{bmatrix} \right\}. \tag{9}$$

BSCs in the substrate can be easily obtained by examining Eq. (6). The presented expressions of SOFs [Eq. (8)] and their BSCs [Eq. (9)] have simple analytic forms, which will make them useful for studying scattering of particles near a substrate, which we further discuss in the next section.

V. SCATTERING BY STRUCTURED OPTICAL FIELDS

Here, scattering calculations are performed for a dielectric sphere on a substrate illuminated by structured Bessel beams. For benchmark purposes, a semianalytic calculation based on the T-matrix method is compared against fully numerical calculation based on finite element analysis. For the T-matrix method, the substrate-mediate coupling should be considered even for a single particle scattering problem. The direct scattering from a particle reflects from the interface, and this reflection acts as a secondary excitation field for the particle. This process involves the evaluation of Sommerfeld-type integrals, which is the main technical difficulty of scattering in stratified media. Refer to Refs. [33–35] for detailed calculation methods. For the finite element analysis, the scattered fields are numerically calculated using the background fields given by Eq. (8). The Maxwellian background fields are readily implemented in finite element analysis solvers. Note that scattered field calculation without any structures should result

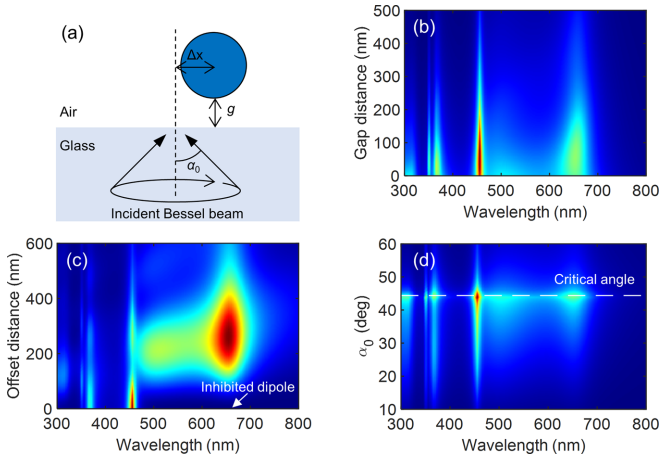

FIG. 4. Parametric studies on scattering of a dielectric sphere on a substrate illuminated by a circularly symmetric Bessel beam. (a) Schematic illustration of the scattering configuration. (b) Multipole strength depending on the gap distance g. The particle is at $\mathbf{r}_p = (80\,\text{nm}, 50\,\text{nm}, g + R)$. (c) Multipole strength depending on the offset distance Δx. The particle is at $\mathbf{r}_p = (\Delta x, 0, 100\,\text{nm})$. (d) Multipole strength depending on the inclination angle α_0. The particle is at $\mathbf{r}_p = (80\,\text{nm}, 50\,\text{nm}, 100\,\text{nm})$. The inclination angle α_0 is 45° for (b) and (c); the polarization state is $(p_x, p_y) = (1, i)/\sqrt{2}$.

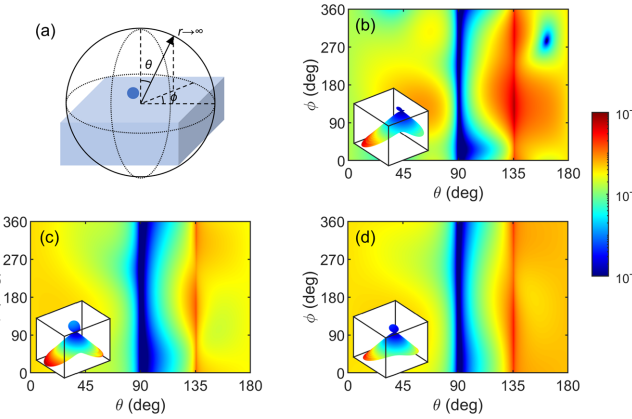

FIG. 5. (a) Schematic illustration of the far-field scattering configuration. (b)–(d) Far-field radiation patterns at wavelengths (b) 450 nm, (c) 500 nm, and (d) 650 nm. The radial part of power flow normalized by the sphere circular area $\hat{\mathbf{r}} \cdot \frac{1}{2}\text{Re}(\mathbf{E} \times \mathbf{H})/(\pi R^2)$ is plotted at $r = 1$ m.

in no scattered fields; this property can be used to confirm if the background fields satisfy Maxwell's equations. The excited multipoles are computed from the localized induced current densities [36,37]. The semianalytic scattering calculations were performed using MATLAB R2021b, and the finite element analysis was performed using COMSOL MULTIPHYSICS 6.0.

First, we examine multipole-decomposed scattering of a dielectric sphere on a substrate illuminated by an evanescent vortex Bessel beam, where the sphere is positioned off axis for benchmark purposes (Fig. 3). The semianalytically calculated results (solid lines) and numerically calculated results (dots) show excellent agreement [Fig. 3(b)]. Here, the semianalytical calculation took around 0.33 s and the finite element analysis took around 64 s using a desktop with its CPU AMD Ryzen 3900X. This factor 200 speedup shows that parametric studies or optimizations can be performed. We further compare the near fields calculated semianalytically [Fig. 3(c)] and numerically [Fig. 3(d)]. The near fields consist of background and scattered fields. The scattered fields in the superstrate consist of direct radiation from the scattering particle and reflection from the interface, and the scattered fields in the substrate are described by the refracted fields from the interface. The near fields calculated semianalytically and numerically show excellent agreement.

The numerical efficiency of the T-matrix method allows us to run parametric studies. To demonstrate this capability, scattering calculations were performed for a dielectric sphere at different positions with respect to the SOF [Fig. 4(a)]. First, we analyze the scattering as the sphere moves away from the substrate [Fig. 4(b)]. The sphere is located at $\mathbf{r}_p = (80\,\text{nm}, 50\,\text{nm}, g + R)$, where g is the gap distance between the substrate and the sphere, and $R = 90\,\text{nm}$ is the sphere radius. As expected from the evanescent SOF, scattering weakens as the sphere moves away from the substrate. We also analyze the scattering as the sphere moves away from the beam center [Fig. 4(c)]. The sphere is located at $\mathbf{r}_p = (\Delta x, 0, 100\,\text{nm})$, where Δx is the offset distance from the beam center to the sphere center. When the beam center $\Delta x = 0$, dipolar resonances are inhibited and only higher-order multipole resonances are observed. As the sphere moves away from the center, the inhibited dipole resonances at wavelength 500–700 nm become stronger. The dipole resonance is strong at offset distance 200–300 nm, where the doughnut-shaped beam has maximum intensity [Fig. 3(d)]. Finally, we analyze the scattering as the Bessel beam inclination angle changes [Fig. 4(d)]. Interestingly, the scattering becomes strong near the critical angle $\theta_c = \arcsin(n_2/n_1) \approx 44.37°$.

A potentially useful application of the T-matrix method for scattering calculations involving stratified media is far-field calculation. Far-field scattering analysis in homogeneous media has widely been performed using the Stratton-Chu formula [38], but the far-field calculation in stratified media requires more complicated steps [39]. On the other hand, the T-matrix method allows efficient evaluation of far-field radiation using the stationary phase approximation [40], which assumes that the wave vector parallel to the propagation direction should be dominant in the far fields. Interestingly, strong emission is observed at the critical angle $\theta = \pi - \theta_c \approx 135.6°$ (Fig. 5). This phenomenon has been reported from the radiation of electric dipole or multipole sources near substrate [41,42]. In addition, transmission at an anticritical angle [43] is observed at $\pi/2 < \theta < \pi - \theta_c$, where propagating plane waves cannot access (Fig. 5). The evanescent part of scattering contributes to this transmission at anticritical angles. This example illustrates that the existence of substrate can strongly modify the emission and scattering properties.

VI. CONCLUSIONS

In this paper, we provide formulations of circularly symmetric SOFs propagating through stratified media [Eq. (5)] and their BSCs [Eq. (6)]. Specifically, the simplest case

of SOFs propagating through a single interface is analyzed [Eq. (7)], which results in a simple analytic expression for Bessel beams [Eq. (8)] and their BSCs [Eq. (9)]. These exact expressions on SOFs propagating through stratified media will provide more accurate results for many realistic scattering configurations encountered in experiments that include substrate, spacer, or finite encapsulation layer. Also, various SOFs can be described including vortex beams, cylindrical vector beams, and evanescent beams that provide many distinct scattering configurations. In addition, the numerical efficiency of T-matrix method is discussed, which significantly extends the applications into optimization and design problems. Especially, this approach can rigorously treat scattering problems involving a large number of particles [44], which could not be considered using conventional numerical tools. Recently, this multipole-based approach has been used to treat random disordered metasurfaces [45] and multiscale problems involving molecules [46].

In addition, more diverse optical effects could be investigated by incorporating stratified media, because the effective polarizability of scattering particles can be modified near the substrate or stratified media. For instance, quasiguided mode resonances depend sensitively on the substrate, and the symmetry of particles could be broken by the existence of substrates. Also, optical coupling between resonant modes of scatterers and layers could be studied for scatterers on plasmonic or polaritonic films.

ACKNOWLEDGMENTS

This work was financially supported by the POSCO-POSTECH-RIST Convergence Research Center program funded by POSCO, and the National Research Foundation (NRF) (Grants No. NRF-2019R1A2C3003129, No. CAMM-2019M3A6B3030637, No. NRF-2019R1A5A8080290, and No. NRF-2022K1A3A1A25081970) funded by the Ministry of Science and ICT of the Korean government. J.M. acknowledges the POSTECH PIURI fellowship and the NRF postdoctoral fellowship (Grant No. NRF-2021R1A6A3A01087429) funded by the Ministry of Education of the Korean government. H.K. acknowledges the POSTECH Alchemist fellowship.

APPENDIX A: CYLINDRICAL VECTOR BEAMS

Cylindrical vector beams can be considered by exchanging (p_x, p_y) with $p_\rho(\cos\beta, \sin\beta) + p_\phi(-\sin\beta, \cos\beta)$ that results in $A_p = p_\rho$ and $A_s = p_\phi$, where p_ρ and p_ϕ correspond to the radial and azimuthal polarizations, respectively. Following the same procedure above, the partial cylindrical waves for cylindrical vector beams are obtained as

$$\tilde{\mathbf{e}}_p(\alpha) = p_\rho \pi i^l e^{il\phi} \begin{bmatrix} \cos\alpha[ie^{i\phi}J_{l+1}(\sigma) - ie^{-i\phi}J_{l-1}(\sigma)] \\ \cos\alpha[e^{i\phi}J_{l+1}(\sigma) + e^{-i\phi}J_{l-1}(\sigma)] \\ -2\sin\alpha J_l(\sigma) \end{bmatrix},$$
$$\tilde{\mathbf{e}}_s(\alpha) = p_\phi \pi i^l e^{il\phi} \begin{bmatrix} e^{i\phi}J_{l+1}(\sigma) + e^{-i\phi}J_{l-1}(\sigma) \\ ie^{i\phi}J_{l+1}(\sigma) - ie^{-i\phi}J_{l-1}(\sigma) \\ 0 \end{bmatrix}. \quad \text{(A1)}$$

Here, the radially and azimuthally polarized modes correspond to p and s polarized modes, respectively.

APPENDIX B: SPHERICAL VECTOR WAVE FUNCTIONS AND MULTIPOLE EXPANSION

Electromagnetic fields satisfying Maxwell's equations in a homogeneous media can be decomposed in terms of the regular spherical vector wave functions as

$$\mathbf{E}(\mathbf{r}) = \sum_{n=1}^{\infty} \sum_{m=-n}^{n} \left[a_{nm}^{\mathrm{e}} \mathbf{N}_{nm}^{(1)}(\mathbf{r}) + a_{nm}^{\mathrm{m}} \mathbf{M}_{nm}^{(1)}(\mathbf{r}) \right], \quad \text{(B1)}$$

where a_{nm}^{e} and a_{nm}^{m} are the electric and magnetic parts of multipole coefficients, respectively, and $\mathbf{N}_{nm}^{(1)}$ and $\mathbf{M}_{nm}^{(1)}$ are the electric and magnetic parts of spherical vector wave functions. The expressions of the basis vary by the literature, and our choice is

$$\mathbf{M}_{nm}^{(1)}(\mathbf{r}) = i\gamma_{nm} j_n(kr)[i\pi_{nm}(\theta)\hat{\theta} - \tau_{nm}(\theta)\hat{\phi}]e^{im\phi},$$
$$\mathbf{N}_{nm}^{(1)}(\mathbf{r}) = \frac{1}{k}\nabla \times \mathbf{M}_{nm}^{(1)}(\mathbf{r}), \quad \text{(B2)}$$

where $j_n(x)$ is the spherical Bessel function of the first kind. The multipole coefficients can be obtained as [47]

$$\begin{bmatrix} a_{nm}^{\mathrm{e}} \\ a_{nm}^{\mathrm{m}} \end{bmatrix} j_n(kr) = -\frac{ik}{E_0\sqrt{n(n+1)}} \int Y_{nm}^*(\hat{r}) \begin{bmatrix} \mathbf{r}\cdot\mathbf{E} \\ i\eta\mathbf{r}\cdot\mathbf{H} \end{bmatrix} d\Omega, \quad \text{(B3)}$$

where $Y_{nm}(\theta, \phi)$ is the spherical harmonics.

APPENDIX C: DERIVATION OF EQ. (6)

Equation (6), or BSCs of Eq. (5), can be evaluated by inserting the cylindrical waves [Eq. (5)] into Eq. (B3) following the procedure in Ref. [29]. Here, we provide an alternative approach that decomposes plane waves [Eq. (4)]. We start from plane wave propagation in a stratified media expressed as

$$\mathbf{E}(\mathbf{r}) = E_0 e^{i\mathbf{k}_\parallel\cdot\mathbf{r}} \sum_{q=p,s} \left[c_{iq}\mathbf{e}_q e^{ik_{iz}z'} + c_{iq}^{(-)}\mathbf{e}_q^{(-)} e^{-ik_{iz}z'} \right], \quad \text{(C1)}$$

the BSCs of which are evaluated as

$$\begin{aligned} \begin{bmatrix} a_{nm}^{\mathrm{e}} \\ a_{nm}^{\mathrm{m}} \end{bmatrix} &= -4\pi\gamma_{nm} i^n e^{-im\beta} e^{i\mathbf{k}_\parallel\cdot\mathbf{r}_p} \\ &\times \left\{ \left[c_{ip} \begin{bmatrix} \tau_{nm}(\alpha_i) \\ \pi_{nm}(\alpha_i) \end{bmatrix} + c_{is} \begin{bmatrix} -i\pi_{nm}(\alpha_i) \\ -i\tau_{nm}(\alpha_i) \end{bmatrix} \right] e^{ik_{iz}z'_p} \right. \\ &+ (-1)^{n+m} \left[c_{ip}^{(-)} \begin{bmatrix} \tau_{nm}(\alpha_i) \\ -\pi_{nm}(\alpha_i) \end{bmatrix} \right. \\ &\left. \left. + c_{is}^{(-)} \begin{bmatrix} -i\pi_{nm}(\alpha_i) \\ i\tau_{nm}(\alpha_i) \end{bmatrix} \right] e^{-ik_{iz}z'_p} \right\}. \end{aligned} \quad \text{(C2)}$$

This expression shares the same functional form with the transformation coefficients of spherical wave expansion of plane waves, and the sign changes of backward propagating waves come from the parity of spherical harmonics. BSCs of Eq. (4) in two-dimensional integral form can be easily ob-

tained by referring to Eq. (C2), from which the simplification with respect to β can be performed by noting that $c_{iq} = \tilde{c}_{iq} A_q$, $A_p(\beta) = e^{i\beta} p_+ + e^{-i\beta} p_-$, and $A_s(\beta) = ie^{i\beta} p_+ - ie^{-i\beta} p_-$, resulting in Eq. (6).

[1] W. Liu and Y. S. Kivshar, Multipolar interference effects in nanophotonics, Phil. Trans. R. Soc. A **375**, 20160317 (2017).

[2] J. Mun, M. Kim, Y. Yang, T. Badloe, J. Ni, Y. Chen, C.-W. Qiu, and J. Rho, Electromagnetic chirality: from fundamentals to nontraditional chiroptical phenomena, Light Sci. Appl. **9**, 139 (2020).

[3] A. Forbes, M. de Oliveira, and M. R. Dennis, Structured light, Nat. Photonics **15**, 253 (2021).

[4] L. Cicchitelli, H. Hora, and R. Postle, Longitudinal field components for laser beams in vacuum, Phys. Rev. A **41**, 3727 (1990).

[5] Y. Shen, X. Wang, Z. Xie, C. Min, X. Fu, Q. Liu, M. Gong, and X. Yuan, Optical vortices 30 years on: OAM manipulation from topological charge to multiple singularities, Light Sci. Appl. **8**, 90 (2019).

[6] Q. Zhan, Cylindrical vector beams: From mathematical concepts to applications, Adv. Opt. Photonics **1**, 1 (2009).

[7] R. M. Kerber, J. M. Fitzgerald, D. E. Reiter, S. S. Oh, and O. Hess, Reading the orbital angular momentum of light using plasmonic nanoantennas, ACS Photonics **4**, 891 (2017).

[8] I. A. Litvin, N. S. Mueller, and S. Reich, Selective excitation of localized surface plasmons by structured light, Opt. Express **28**, 24262 (2020).

[9] A. G. Lamprianidis and A. E. Miroshnichenko, Excitation of nonradiating magnetic anapole states with azimuthally polarized vector beams, Beilstein J. Nanotechnol. **9**, 1478 (2018).

[10] S. Reich, N. S. Mueller, and M. Bubula, Selection rules for structured light in nanooligomers and other nanosystems, ACS Photonics **7**, 1537 (2020).

[11] P. Woźniak, P. Banzer, and G. Leuchs, Selective switching of individual multipole resonances in single dielectric nanoparticles, Laser Photonics Rev. **9**, 231 (2015).

[12] K. Sakai, K. Nomura, T. Yamamoto, and K. Sasaki, Excitation of multipole plasmons by optical vortex beams, Sci. Rep. **5**, 8431 (2015).

[13] X. Zambrana-Puyalto, X. Vidal, P. Woźniak, P. Banzer, and G. Molina-Terriza, Tailoring multipolar mie scattering with helicity and angular momentum, ACS Photonics **5**, 2936 (2018).

[14] R. Kerber, J. Fitzgerald, S. Oh, D. Reiter, and O. Hess, Orbital angular momentum dichroism in nanoantennas, Commun. Phys. **1**, 87 (2018).

[15] R. Masoudian Saadabad, M. Cai, F. Deng, L. Xu, and A. E. Miroshnichenko, Structured light excitation of toroidal dipoles in dielectric nanodisks, Phys. Rev. B **104**, 165402 (2021).

[16] L. Wei, Z. Xi, N. Bhattacharya, and H. P. Urbach, Excitation of the radiationless anapole mode, Optica **3**, 799 (2016).

[17] J. A. Parker, H. Sugimoto, B. Coe, D. Eggena, M. Fujii, N. F. Scherer, S. K. Gray, and U. Manna, Excitation of Nonradiating Anapoles in Dielectric Nanospheres, Phys. Rev. Lett. **124**, 097402 (2020).

[18] Y. Lu, Y. Xu, X. Ouyang, M. Xian, Y. Cao, K. Chen, and X. Li, Cylindrical vector beams reveal radiationless anapole condition in a resonant state, Opto-Electron. Adv. **5**, 210014 (2022).

[19] K. Koshelev, S. Kruk, E. Melik-Gaykazyan, J.-H. Choi, A. Bogdanov, H.-G. Park, and Y. Kivshar, Subwavelength dielectric resonators for nonlinear nanophotonics, Science **367**, 288 (2020).

[20] T. Das, P. P. Iyer, R. A. DeCrescent, and J. A. Schuller, Beam engineering for selective and enhanced coupling to multipolar resonances, Phys. Rev. B **92**, 241110(R) (2015).

[21] K. Y. Bliokh, A. Y. Bekshaev, and F. Nori, Extraordinary momentum and spin in evanescent waves, Nat. Commun. **5**, 3300 (2014).

[22] P. C. Chaumet, Fully vectorial highly nonparaxial beam close to the waist, J. Opt. Soc. Am. A **23**, 3197 (2006).

[23] T. Nieminen, H. Rubinsztein-Dunlop, and N. Heckenberg, Multipole expansion of strongly focussed laser beams, J. Quant. Spectrosc. Radiat. Transfer **79–80**, 1005 (2003).

[24] A. A. R. Neves, A. Fontes, L. A. Padilha, E. Rodriguez, C. H. de Brito Cruz, L. C. Barbosa, and C. L. Cesar, Exact partial wave expansion of optical beams with respect to an arbitrary origin, Opt. Lett. **31**, 2477 (2006).

[25] W. L. Moreira, A. A. R. Neves, M. K. Garbos, T. G. Euser, and C. L. Cesar, Expansion of arbitrary electromagnetic fields in terms of vector spherical wave functions, Opt. Express **24**, 2370 (2016).

[26] J. Mun, S.-W. Moon, and J. Rho, Multipole decomposition for interactions between structured optical fields and meta-atoms, Opt. Express **28**, 36756 (2020).

[27] J. J. Wang, T. Wriedt, J. A. Lock, and L. Mädler, General description of circularly symmetric bessel beams of arbitrary order, J. Quant. Spectrosc. Radiat. Transfer **184**, 218 (2016).

[28] J. J. Wang, T. Wriedt, J. A. Lock, and Y. C. Jiao, General description of transverse mode bessel beams and construction of basis bessel fields, J. Quant. Spectrosc. Radiat. Transfer **195**, 8 (2017).

[29] J. J. Wang, T. Wriedt, L. Mädler, Y. P. Han, and P. Hartmann, Multipole expansion of circularly symmetric bessel beams of arbitrary order for scattering calculations, Opt. Commun. **387**, 102 (2017).

[30] L. Allen, M. W. Beijersbergen, R. J. C. Spreeuw, and J. P. Woerdman, Orbital angular momentum of light and the transformation of Laguerre-Gaussian laser modes, Phys. Rev. A **45**, 8185 (1992).

[31] D. M. Marques, J. A. Guggenheim, R. Ansari, E. Z. Zhang, P. C. Beard, and P. R. Munro, Modelling fabry-pérot etalons illuminated by focussed beams, Opt. Express **28**, 7691 (2020).

[32] S. Mei, K. Huang, T. Zhang, M. Q. Mehmood, H. Liu, C. T. Lim, J. Teng, and C.-W. Qiu, Evanescent vortex: Optical subwavelength spanner, Appl. Phys. Lett. **109**, 191107 (2016).

[33] M. Paulus, P. Gay-Balmaz, and O. J. F. Martin, Accurate and efficient computation of the Green's tensor for stratified media, Phys. Rev. E **62**, 5797 (2000).

[34] A. Egel, S. W. Kettlitz, and U. Lemmer, Efficient evaluation of Sommerfeld integrals for the optical simulation of many scattering particles in planarly layered media, J. Opt. Soc. Am. A **33**, 698 (2016).

[35] K. M. Czajkowski, M. Bancerek, and T. J. Antosiewicz, Multipole analysis of substrate-supported dielectric nanoresonator metasurfaces via the t-matrix method, Phys. Rev. B **102**, 085431 (2020).

[36] P. Grahn, A. Shevchenko, and M. Kaivola, Electromagnetic multipole theory for optical nanomaterials, New J. Phys. **14**, 093033 (2012).

[37] J. Mun, S. So, J. Jang, and J. Rho, Describing meta-atoms using the exact higher-order polarizability tensors, ACS Photonics **7**, 1153 (2020).

[38] J. A. Stratton and L. Chu, Diffraction theory of electromagnetic waves, Phys. Rev. **56**, 99 (1939).

[39] J. Yang, J.-P. Hugonin, and P. Lalanne, Near-to-far field transformations for radiative and guided waves, ACS Photonics **3**, 395 (2016).

[40] W. Chew, A quick way to approximate a Sommerfeld-Weyl-type integral (antenna far-field radiation), IEEE Trans. Antennas Propag. **36**, 1654 (1988).

[41] W. Lukosz, Light emission by magnetic and electric dipoles close to a plane dielectric interface. iii. radiation patterns of dipoles with arbitrary orientation, J. Opt. Soc. Am. **69**, 1495 (1979).

[42] H. F. Arnoldus, Power emitted by a multipole near an interface, Surf. Sci. **571**, 173 (2004).

[43] H. F. Arnoldus and J. T. Foley, Transmission of dipole radiation through interfaces and the phenomenon of anti-critical angles, J. Opt. Soc. Am. A **21**, 1109 (2004).

[44] J. Skarda, R. Trivedi, L. Su, D. Ahmad-Stein, H. Kwon, S. Han, S. Fan, and J. Vučković, Low-overhead distribution strategy for simulation and optimization of large-area metasurfaces, npj Comput. Mater. **8**, 78 (2022).

[45] A. Rahimzadegan, D. Arslan, R. N. S. Suryadharma, S. Fasold, M. Falkner, T. Pertsch, I. Staude, and C. Rockstuhl, Disorder-Induced Phase Transitions in the Transmission of Dielectric Metasurfaces, Phys. Rev. Lett. **122**, 015702 (2019).

[46] B. Zerulla, M. Krstić, D. Beutel, C. Holzer, C. Wöll, C. Rockstuhl, and I. Fernandez-Corbaton, A multi-scale approach for modeling the optical response of molecular materials inside cavities, Adv. Mater. **34**, 2200350 (2022).

[47] J. D. Jackson, *Classical Electrodynamics*, 3rd ed. (Wiley, New York, 1999).